

ACOUSTIC INVERSION FOR GAS BUBBLE DISTRIBUTIONS IN MARINE SEDIMENTS: MERCURY RESULTS

H Dogan Institute of Sound and Vibration Research, Uni. Southampton, Southampton, UK
PR White Institute of Sound and Vibration Research, Uni. Southampton, Southampton, UK
TG Leighton Institute of Sound and Vibration Research, Uni. Southampton, Southampton, UK

1 INTRODUCTION

Gas is a common occurrence in deep sea as well as in organic-rich, muddy sediments of coastal waters and shallow seas¹. The depths and horizontal distributions of these gas-charged sediments are usually detected from seismic profiling.

According to Anderson *et al.*², bubbly sediments can be separated into three types. The first type is the interstitial bubbles, in which the gas bubble size is smaller than the interstitial spaces of the sediment skeletal frame. Such bubbles may either float in the pore water or adhere to walls of a pore space. The second type is the gas reservoir, where the sediment framework remains essentially unaltered by the free gas. This type of bubbles has sizes greater than the pore space. The third type, the sediment displacing bubble, in which the sediment framework is deformed actually, displaced by the bubble.

Typically acoustic bubble sizing techniques employ resonance characteristics of bubbles which pulsate under insonification. These are classified in two broad categories. The first one employs transmission measurements (i.e. measurements of speed and attenuation of sound waves propagating through a bubbly medium) whilst the second one uses (back) scattering measurements to infer the bubble size distributions³.

Current acoustic systems are effective in gas detection⁴ but not in quantification of the gas present or providing shape information of the gas voids in the sediment. Recent scientific research suggests that it is possible to relate the acoustic transmission measurements with bubble sizes^{5, 6}. However to date there is no acoustic method able to give information about the gas shape without supporting CT scanning images. Both the shape and size of the gas voids are important because they influence the sediment loading capacity and stability. The present study aims towards the development of an acoustic system able to both detect and quantify the gas present in marine sediments.

2 THEORY

2.1 Forward problem statement

The most common approach when dealing with the forward problem of bubble dynamics is to introduce the well-known linearization procedure assuming small amplitude variations of the bubble wall, i.e. $R = R_0(1 + x)$ where $x \ll 1$, and from that to derive the damping coefficients, scattering cross-section, sound speed and attenuation expressions. Such linear models are especially useful when the driving pressure amplitudes are low. For our current purposes, we proceed with the linear formulation the reasons for that being twofold: (i) the acoustic transducers which we also tested in water tank experiments are operated at low pressure amplitudes and (ii) the acoustic inversion method which is described in the next section and adapted for a viscoelastic medium for the first time essentially uses linear the extinction cross-section of bubbles. For the method developed in this article we skip the details regarding the expressions for the linear damping coefficients, attenuation

due to individual bubbles and the collective speed of sound formula, and turn our attention to the scattering and the extinction cross-sections.

A recent study⁷ has shown that the commonly encountered expressions, regardless of either using the dimensional form of the damping coefficients or the non-dimensional form, for the scattering and extinction coefficients involve errors on how the radiation damping enters the derivations. Accordingly, the corrected scattering cross-section of a bubble is given as

$$\sigma_s = \frac{4\pi R_0^2}{\left(\frac{\omega_0^2}{\omega^2} - 1 - 2\frac{\beta_0}{\omega} \varepsilon\right)^2 + \left(2\frac{\beta_0}{\omega} + \frac{\omega_0^2}{\omega^2} \varepsilon\right)^2} \quad (1)$$

where β_0 is the total of the damping coefficients other than acoustic damping, e. g. viscous, thermal, elastic and interfacial damping. The expression for the extinction cross-section reads:

$$\sigma_e = \sigma_s \left(1 + \frac{2\beta_0/\omega}{\varepsilon}\right) \quad (2)$$

where $\varepsilon \equiv \omega R_0/c$.

2.2 Inverse problem

The previously developed method by Commander and McDonald⁸ for the determination of bubbles size distributions in water is adapted for the case of bubble size distributions in marine sediments. The mathematical nature of the problem is the same as the former one provided that the additional physical processes encountered owing to the elasticity of the sediment are accounted for. Accordingly, the stability and the accuracy of the inversion scheme is affected by these physics as explained in the following.

The attenuation of an acoustic plane wave caused by a bubble population with a range of radii (R_{\min} , R_{\max}) is governed by the following Fredholm integral equation of the first kind

$$\alpha(f) = \int_{R_{\min}}^{R_{\max}} \sigma_e(f, R_0) \Psi(R_0) dR_0 \quad (3)$$

where $\alpha(f)$ is the measured attenuation at the applied frequency f , Ψ is the unknown bubble distribution and σ_e is the extinction cross-section defined in the previous section. The applied frequency, in general, should cover the resonance range of the minimum and the maximum bubble sizes present in the medium. The solution of Eq. (3) is performed by expanding the unknown bubble distribution by a finite sum of linear B -splines, i.e.

$$\Psi(R) = \sum_{j=1}^N \Psi_j B_j(R) \quad (4)$$

where Ψ_j is the value of the function Ψ at point R_0 and B_j is the j th B -spline. The above expansion, in principal, allows the use of an adaptive grid for the bubble distribution. Substitution of (4) into (3) yields a linear set of equations:

$$\alpha(f_i) = \sum_{j=1}^N K_{ij} \Psi_j \quad (5)$$

where the elements of the matrix kernel are given by

$$K_{ij} = \int_{R_{\min}}^{R_{\max}} \sigma_e(f_i, R_0) B_j(R_0) dR_0. \quad (6)$$

In matrix notation, Eq. (6) may be written as

$$\begin{pmatrix} K_{11} & K_{12} & K_{13} & \cdots & K_{1N} \\ K_{21} & K_{22} & K_{23} & \cdots & K_{2N} \\ K_{31} & K_{32} & K_{33} & \cdots & K_{3N} \\ \vdots & \vdots & \vdots & & \vdots \\ K_{N1} & K_{N2} & K_{N3} & \cdots & K_{NN} \end{pmatrix} \begin{pmatrix} \Psi_1 \\ \Psi_2 \\ \Psi_3 \\ \vdots \\ \Psi_N \end{pmatrix} = \begin{pmatrix} \alpha_1 \\ \alpha_2 \\ \alpha_3 \\ \vdots \\ \alpha_N \end{pmatrix}. \quad (7)$$

Note that since the j th linear B -spline is only non-zero at the neighboring indices $j-1$ and $j+1$, the actual limits of the integral equation (6) are the values of R at these points. The integral equation in (6) for each matrix kernel is computed using a 10-point Gauss-Legendre quadrature.

The resulting system (7) is, in general, ill-conditioned which may be a combination of several factors such as the large values of off-diagonal elements, the choice of the increments in bubbles size, i.e. uniform or adaptive, the match of the range values of the applied frequencies and the bubble radii, and the number of measurements N . The advantage of the singular value decomposition (SVD) is that further regularization techniques may be applied in order to overcome the instabilities caused by small singular values of the system⁸. The regularization method is based on the smoothness and minimum curvature constraints; the resulting system is expressed as

$$(K^T K + \lambda D^T D) \Psi = K^T \alpha \quad (8)$$

where λ is the regularization parameter. The operator D imposes second order difference (the explicit form is defined in their paper and references therein) which ensures the above mentioned constraints; thus discontinuities in the inverted bubble distribution profile are not observed.

In order to confirm the validity of the developed method, inversion computations with known analytical solutions can be performed. The underlying idea behind this is that for a known bubble size distribution, a range of insonifying frequency and the physical properties of the sediment, the attenuation profile is known. Using the obtained attenuation profile as a measured set of data, one may solve the inverse problem in order to investigate the range of the regularization parameter. The inversion method is tested for the triangular bubble size distribution and the results are shown in Fig. 1. The effects of the regularization parameter are observed as follows. For small values of λ , the inverted bubble population includes negative values which are unphysical and for $\lambda = 1$ the obtained profile exhibits large deviations from the triangular distribution. Large values of λ imposes a constraint on the solution towards a straight line⁸, as observed in Fig. 1 for $\lambda = 10^5$. In the case real attenuation data, the selection of λ would be more critical since the measurement data would not be as smooth as given by analytical functions and would rather include additional noise. Note that Commander and McDonald⁸ do not present any robust selection criteria for the final choice of λ for an arbitrary measurement data. In this work, a L-curve minimization method is applied, the details of which can be found in Leighton et. al⁹.

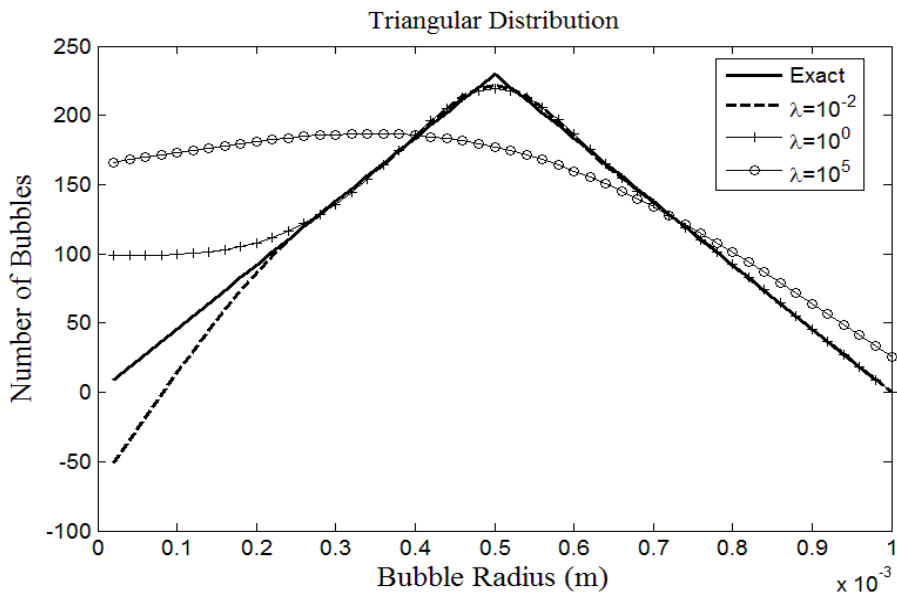


Figure 1: The effect of the regularization parameter on the stability of the inverted bubble populations.

3 EXPERIMENTAL SETUP

The experimental rig used in the work reported here consists of 5 acoustical components, i.e. one source transducer and four hydrophones, mounted on aluminum bars. The propagation rig is designed so that the source to receiver separations can be adjusted for the sediment type under examination, e.g. in saturated muds much larger S-R separations can be used than in gassy muds. In order to achieve this, it has been constructed using 30 mm long aluminum struts. These receiver clamps are capable of sliding along the 2 m long main strut and are attached with T bar connectors. The rig further comprises two 0.5 m stabilizing bars. It is inserted into the sediment with a 45° angle (see Fig. 2); the corresponding spreading losses at this angle are accounted for during the processing stage.

The acoustic source, from Neptune Sonar, consists of three elements and operates in 25-120 kHz frequency range. The source and the wet end was matched by Blacknor Technology and is contained in a pressure cylinder approximately 0.6 m from the transducer. Although initial calibration documents were received, additional calibrations of source levels were performed in order to include the effects of the wet end matching. A BLK 1264 pump amplifier with a 3.5 V peak to peak voltage input was used in calibration tests. The measured source levels varied from 200 to 213 dB re $\mu\text{Pa}/3.5\text{ V}$ at 1m distance for 25-120 kHz frequency range.

The receivers are four modified D140 hydrophones (Neptune Sonar). The main difference between the standard D140s and the modified devices is the material encasing the hydrophone element, which has been modified to supply additional protection for insertion into sediment. The sensitivity of the receivers varied from -209 to -217 dB re $1\text{V}/\mu\text{Pa}$ from 26 to 100 kHz. These hydrophones have been attached to carbon fibre poles manufactured by Tricast with the acoustic centre of the hydrophone element lying 0.55 m from the end of the pole. The hydrophones have a wet end amplifier which was supplied by the producer approximately 0.5 m from the receiver. Amplification is applied at both the wet and dry ends in three stages with adjustable gains. Trial transmission tests confirmed that the timing of the acquisition system was reliable to the sampling period of the acquisition card (1 μs) and the amplitude was reliable to the voltage resolution of the card (2.5 mV).

The rig was deployed at muddy sites and river bays near the Southampton Harbour area,

Hampshire U.K. The procedure involved determining the experiment location within 20 m of dry point for acquisition system. A triangular hole was cut through which the source probe and the hydrophone array is inserted into the sediment at a near 45° (46.5° was also tried in some cases). It was ensured that there is good coupling between the sediment and the acoustic components. The next stages involve setting up the connections with acquisition system and sending out a series of test signals using the acquisition code written in MATLAB software. The source levels, the wet end and dry end receiver gains are changed in order to maximize the signal at receiver. The frequency was increased at 2 kHz steps from 26 kHz to 100 kHz. At each frequency, a number of shots were sent out, i.e. 20, 30 or 40, with relevant pauses in between; this procedure ensures a reliable data set which gives the chance of investigating standard deviation of measured sound speed and attenuation values whilst making the use of stacking and averaging based processing approaches possible. In principle, the data can be analyzed from a combination of different hydrophone pairs, e.g. the pair 1-2, 2-3 or 1-4 etc. The waveform of the input signal was selected as square wave envelope with either 1 ms duration or 20 oscillations.

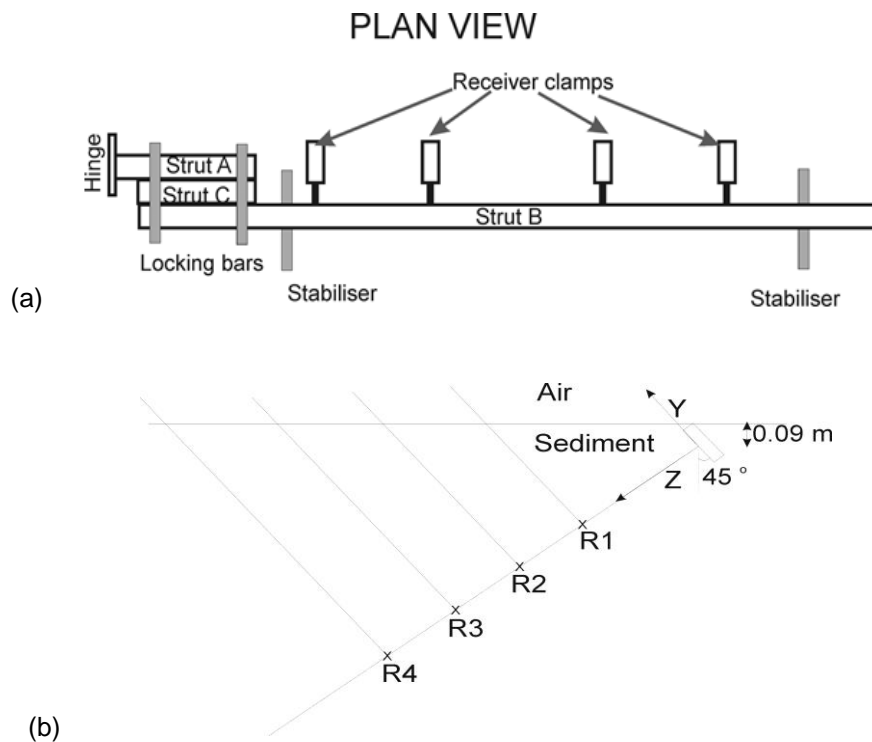


Figure 2: Gassy sediment experiment propagation rig, (a) plan view and (b) *in situ* deployed configuration. R1, R2, R3 and R4 denote the locations of four hydrophone receivers.

4 SIGNAL PROCESSING METHOD

In order to perform an accurate analysis of the measurements, robust signal processing methodologies should be applied to the received signals. A thorough analysis should account for the spreading losses in the sediment, examine the variability of the waves emitted by the source transducer, the variability of the coupling between the sediment and the receiver hydrophones and present a detailed analysis of intrinsic errors.

The receivers used in this experiment are identical and the data is (pre)processed choosing certain receiver pairs; hence this simplifies some of the above mentioned prerequisites. For instance, the coupling between the sediment and the receiver can be taken as equal assuming the physical properties of the sediment such as porosity, mean grain size and silt/clay content do

not change greatly over the length scales encountered in this experiment (~20-40 cm for receiver pairs). Moreover, the time delays incurred by the electronic components of the devices and by the casing of the hydrophones can be regarded as the same since identical receivers are used. The recorded signals are pre-processed in order to increase the signal-to-noise ratios (SNR). The variability of the emitted acoustic waves in this experiment were tested in water tank calibration trials. The FFT results have shown that the central frequency of the output signal from the transducer lies within 1% of the input signal to the function generator device. Further, the received signals exhibited central frequencies within 3% of the transducer output signals. Identical, non-casual pre-processing is applied to each channel not to affect the computed velocity and attenuation values. These preprocessing techniques involve filtering and stacking.

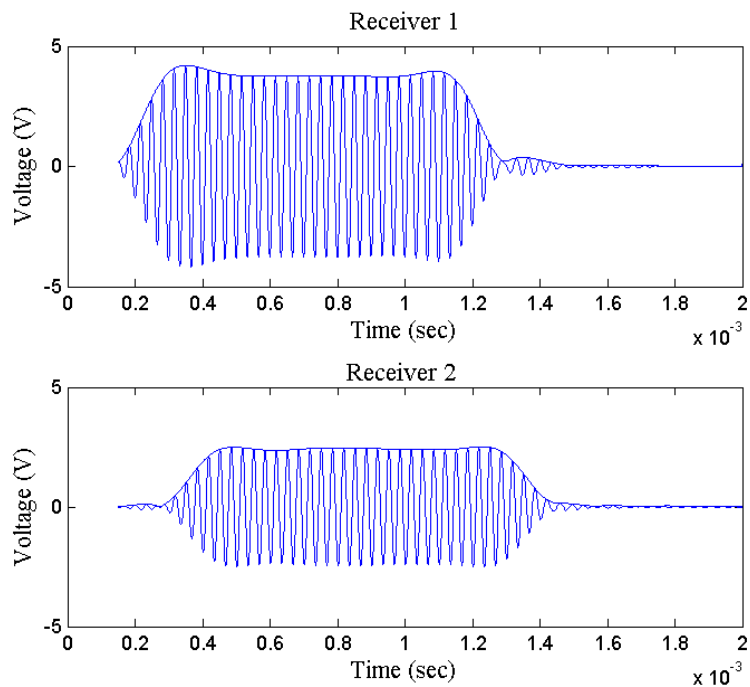


Figure 3: Recorded signals at hydrophone receiver 1 and receiver 2. The data was acquired in Calshot, Southampton UK on 04/08/08. The central frequency is 30 kHz. The shown envelopes are computed by applying Hilbert transform.

The 'useful' energy contained in a pulse can be obtained by evaluating the spectral amplitude of the signal. The general approach is to set lower and upper limits for the frequency band, i.e. the frequencies at which 1% or 10% of the peak spectral amplitude is observed for each insonifying frequency. The power spectral densities were observed to determine the frequencies at which dominant noise events occurred. At central frequencies of 26-30 kHz, noise events occurred at 35 kHz or greater. The majority of the input frequencies used (30-100 kHz) has shown noise events at less than 10 kHz and greater than 300 kHz. Note that different receiver devices out of the selected receiver pairs may have noise distributed to different frequencies; however it was ensured that the major part of the 'useful' energy is retained by applying the same appropriate cut-off frequencies to both receiver signals. Fifth-order Butterworth band-pass filter were used, the band-width of which (varying for each insonifying frequency) was computed from power spectral density. Fig. 3 shows an example of filtered signals recorded at a pair of receivers. The compressional wave velocity of the sediment is evaluated performing time correlation of the signals. To determine the attenuation, the steady part of the signals are identified, then the attenuation is obtained by comparing the decrease of wave amplitudes in these steady parts.

5 RESULTS

In situ and laboratory transmission measurements were carried out using the same materials and methods for the intertidal site named Mercury (N 50° 52' 56", W 001°18' 34). *In situ* attenuation results are shown in Figure 4. The solid line in Fig. 4a represents results from the first hydrophone pair (hydrophone 1 and 2) and the solid line in Fig. 4b from the second hydrophone pair (hydrophones 2 and 3). The first hydrophone pair measured an average *P*-wave sound speed of 1323 m/s and a standard deviation 110 m/s (not shown here). If a linear dependence of attenuation with frequency were to be fitted to these data, then the value of K_P would equal to 0.32 dB/m/kHz. The second hydrophone pair measured an average sound speed of 1250 m/s with a standard deviation of 240 m/s. Assuming, again, a linear dependence of attenuation with frequency, the value of K_P equals 1.1 dB/m/kHz. The values of K_P serve as baselines for comparing attenuation trends between in situ measurements and previous literature.

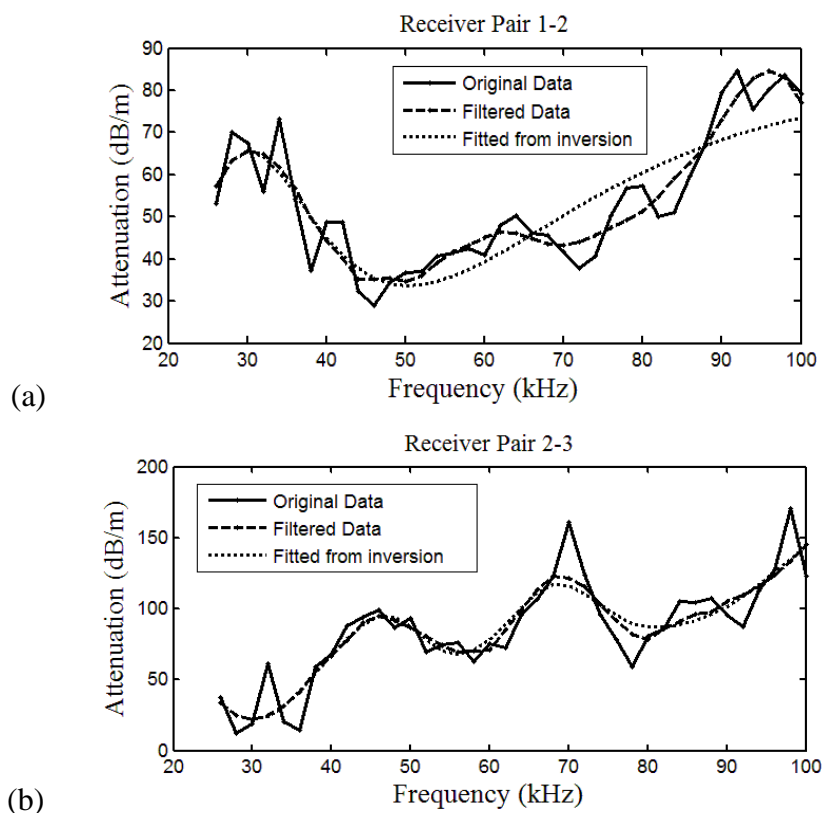


Figure 4: Attenuation profiles as a function of frequency: measured attenuation profiles (original data), processed data used in the inversion algorithm (filtered) and output of the inversion for bubble population (fitted). a) Attenuation data from receiver pair 1-2 and b) attenuation data from receiver pair 2-3.

The inverted bubble populations from the Mercury site are shown in Fig. 5 for hydrophone pair 1-2 and 2-3. A void fraction of 0.66 % is predicted for the pair 1-2 and for hydrophone pair 2-3 a void fraction value of 0.17 %. The regularization parameter λ was determined via the L-curve as 0.0478 for the receiver pair 1-2 and as $2.33 \cdot 10^{-7}$ for receiver pair 2-3.

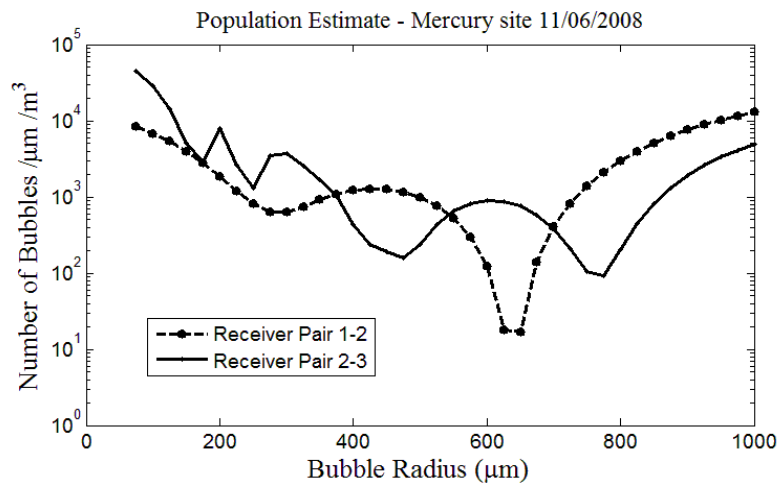


Figure 5: Bubble population results for the Mercury site inverted from receiver pairs 1-2 and 2-3.

6 CONCLUSIONS

A method for estimating the bubble size distribution and bubble void fraction in gassy marine sediments is presented. The method adapts a well-known inversion technique which is widely applied to bubbly waters. First, it is verified by testing analytical results and then applied to measurement data which were acquired via transmission experiments at Mercury site in UK.

7 REFERENCES

1. Judd, A. G., and Hovland, M. (1992). "The evidence of shallow gas in marine sediments" *Continental Shelf Research* 12, 1081-1095.
2. Anderson, A. L., Abegg, F., Hawkins, J. A., Duncan, M. E., and Lyons, A. P. (1998). "Bubble populations and acoustic interaction with the gassy floor of Eckernforde Bay," *Continental Shelf Research* 18, 1807-1838.
3. Clay, C. S., and Medwin, H. (1977). *Acoustical oceanography: principles and applications* (New York: Wiley).
4. Wever, T. F., Abegg, F., Fiedler, H. M., Fechner, G., and Stender, I. H. (1998). "Shallow gas in the muddy sediments of Eckernforde Bay, Germany," *Continental Shelf Research* 18, 1715-1739.
5. Best, A. I., Tuffin, M. D. J., Dix, J. K., and Bull, J. M. (2004). "Tidal height and frequency dependence of acoustic velocity and attenuation in shallow gassy marine sediments," *J. Geophys. Res.* 109.
6. Leighton, T. G., and Robb, G. B. N. (2008). "Preliminary mapping of void fractions and sound speeds in gassy marine sediments from subbottom profiles," *J. Acoust. Soc. Am.* EL313-EL320 124, 313-320.
7. Ainslie, M. A., and Leighton, T. G. (2009). "Near resonant bubble acoustic cross-section corrections, including examples from oceanography, volcanology, and biomedical ultrasound," *J. Acoust. Soc. Am.* 126, 2163-2175.
8. Commander, K., and McDonald, R. J. (1991). "Finite-element solution of the inverse problem in bubble swarm acoustics," *J. Acoust. Soc. Am.* 89, 592-597.
9. Leighton, T. G., Meers, S. D., and White, P. R. (2004). "Propagation through nonlinear time-dependent bubble clouds and the estimation of bubble populations from measured acoustic characteristics" *Proceedings of the Royal Society* 460, 2521-2550.